Electrochemical Defect-Mediated Thin-Film Growth

K. Sieradzki,* S. R. Brankovic, N. Dimitrov

An electrodeposition technique is described that produces atomically flat epitaxial metal overlayers of quality similar to that obtained by ultrahigh vacuum techniques at elevated temperature. In this approach, a metal of interest such as silver is co-deposited with a reversibly deposited mediator metal. The mediator is periodically deposited and stripped from the surface, and this serves to significantly increase the density of two-dimensional islands of silver atoms, promoting a layer-by-layer thin-film growth mode. In situ scanning tunneling microscopy was used to demonstrate the growth process for the heteroepitaxial system silver/gold (111) with either lead or copper as the mediator.

Thin-film deposition is a grail of electrochemistry, yet it is generally viewed as an "art" rather than a science, and to date, the growth of atomically flat epitaxial films to a significant thickness has not been possible. In contrast, ultrahigh vacuum (UHV) techniques for the production of such overlayers are well known, and much progress has been made in recent years in deciphering the underlying physics that controls thin-film growth modes. This improved understanding has led to various discoveries in which the growth kinetics are manipulated to enhance the evolution of an atomically flat overlayer (*1*). We have exploited some of these UHV-derived concepts in developing an electrodeposition technique that produces atomically flat, heteroepitaxial, single-crystal metal overlayers of quality similar to those obtained by elevated-temperature UHV techniques such as molecular beam epitaxy. Conventionally the electrodeposition of metals is carried out in the presence of organic agents that promote so-called "leveling" and "brightening" of the deposited metal, which takes the form of a polycrystalline film (*2, 3*). The formulations of electrolytes containing these agents together with the prescriptions for deposition are highly empirical (*4*).

For a few special metal/metal systems, electrodeposition has been used to grow ultrathin heteroepitaxial overlayers. Magnussen *et al.* showed that for the deposition of Ni on Au(111) substrates epitaxial layer-by-layer growth was obtained to about five monolayers (ML) (*5*). Kolb and co-workers showed that Cu could be deposited on Au(100) (*6*) or Ag(100) (*7*) substrates in a layer-by-layer growth mode up to about 10 ML. The growth regime that we address herein involves considerably thicker overlayers (~250 ML or more). To our knowledge, an electrodeposition process has not been used before to successfully grow such high-quality films in a thickness regime that is of technological significance.

The difficulties in producing flat homoepitaxial or heteroepitaxial overlayers by electrodeposition are similar to those encountered during ambient-temperature vacuum deposition of thin films (*1*). Because of kinetic issues, three-dimensional (3D) growth is often encountered for overlayer/substrate systems that should, according to thermodynamic considerations, grow in a flat 2D mode. Thin-film growth modes are generally classified as Frank–van der Merve or layer-by-layer (2D) growth, Volmer-Weber or 3D cluster growth, and Stranski-Krastanov, which is associated with a transition from 2D to 3D growth. Step-flow growth is a variant of the Frank–van der Merve mode and occurs at an appropriate step density and deposition flux.

The strategy that we used to manipulate the growth kinetics is based on recent UHV deposition experiments that examined Ag/Ag(111) homoepitaxy (*8, 9*). At ambient temperature, because of kinetics, this system displays 3D growth. Rosenfeld *et al.* (*8*) found that by depositing Ag atoms on a substrate with an artificially created high density of Ag clusters, several monolayers of layer-by-layer growth could be induced. This was accomplished by ion bombarding the surface with a low-energy Ar^+ pulse after the completion of each monolayer. Alternatively, van der Vegt *et al.* (*9*) deposited 0.2 ML of Sb that served as a "surfactant" to induce layer-by layer growth of Ag.

Several kinetic models and physical arguments have been developed to explain the results of these experiments (*10–13*). The basic idea is as follows. In order for growth to proceed in a 2D mode, the interlayer transport of deposited adatoms must be rapid, otherwise nucleation of islands occurs on the as yet uncompleted growing monolayers, which can result in 3D growth (*14*). There is a barrier for adatom migration over a descending step that dominates interlayer transport (*15, 16*). The attempt frequency for migration over the barrier is determined by the ratio D/L^2, where D is the adatom diffusivity and L is a length scale characterizing the island size. Analytical arguments predict a critical 2D island radius for the transition to 3D growth of order $(4a^2D/J)^{1/6}$, where J is the deposition flux and a is the near-neighbor hopping distance (*10, 17*). These arguments predict that layer-by-layer growth should occur when the critical island size is greater than the separation between 2D nuclei. Experimental conditions favoring large values of D/L^2 (high temperature) or enhancing nucleation promote 2D growth. Surfactants act to enhance the nucleation density or reduce the magnitude of the edge barrier or both (*10–13*).

We developed an electrochemical technique that serves to significantly enhance the ambient-temperature nucleation of 2D islands. In this approach, which we term electrochemical defect-mediated growth (DMG) (*18*), the metal of interest is co-deposited with a reversibly deposited mediator metal. The mediator is periodically deposited and stripped from the surface by appropriate cycling of the electrochemical potential. Each cycle creates new nuclei on the surface, adding to the existing clusters that developed in previous cycles. A high density of 2D clusters on a growing layer is maintained by the appropriate choice of deposition flux and cycling frequency. A monolayer is completed as the growing 2D clusters eventually merge. A necessary characteristic of the mediator is that it must be electrochemically less noble than the metal of interest.

Using the DMG technique we have successfully grown atomically flat, epitaxial, single-crystal thin films (~150 nm in thickness) for the systems Ag/Ag(111) and Ag/Au(111), which typically display 3D growth at ambient temperature (*19*). Here, we discuss our results for the system Ag/Au(111), which forms two flat wetting layers followed by 3D cluster growth (Stranski-Krastanov growth mode) (*20*). DMG in this system was studied with two different types of mediators: Pb and Cu. Lead is known to underpotentially deposit (upd) on both Au(111) and Ag(111) substrates, and under appropriate potential control, the quantity of Pb deposited is thermodynamically limited to one full-density monolayer (*21–23*).

In situ electrochemical scanning tunneling microscopy (STM) was used to monitor the details of the DMG process. These studies were performed with a Molecular Imaging Pico STM with a model 300S scanner and a

---

Department of Mechanical and Aerospace Engineering, Arizona State University, Tempe, AZ 85287–6106, USA.

*To whom correspondence should be addressed. E-mail: karl@icarus.eas.asu.ed

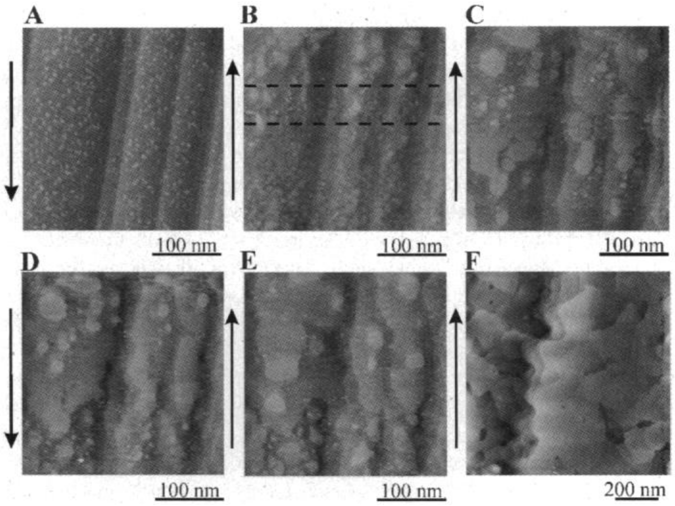

Fig. 1. (A to E) A time sequence of in situ STM images of Pb-mediated growth of Ag in the 0.1 M $HClO_4$ + 4 × 10^{-4} M $AgClO_4$ + 0.1 M $Pb(ClO_4)_2$ electrolyte: (**A**) at 0.756 V, 2D nuclei corresponding to the initial stage of formation of the second Ag wetting layer, 0 s; (**B**) a 6-s potential pulse (the region between the dashed black lines) from 0.350 to 0.050 V and back seeded a third Ag layer, 37 s; (**C**) at 0.050 V, seeding of a fourth layer, 111 s; (**D**) at 0.350 V, 148 s; and (**E**) at 0.350 V, after another 6-s potential pulse that seeded a fifth layer, 185 s. (**F**) A 250-ML-thick Ag overlayer on Au(111), at 0.756 V. Potentials are referenced to the Pb/0.1 M Pb^{2+} reference electrode. Image acquisition time was 26 s. The arrows indicate the scan direction.

Molecular Imaging model 300S Pico Bi-Potentiostat. The STM was operated in the constant-current mode. The STM cell used was made of Teflon and exposed an area of working electrode of 0.30 cm^2 and had a volume of ~1.36 cm^3. This large-volume electrochemical STM cell allowed us to observe the growth of up to ~600 ML of Ag. Before each experiment, an STM tip was prepared by etching an 80:20 Pt + Ir wire in a $CaCl_2$ solution and isolating it with Apiezon wax. Gold (111) single crystals, in the form of 10-mm-diameter disks 2 mm thick, were used as a substrate. The gold surface was prepared before each deposition experiment by electrochemical polishing followed by hydrogen flame annealing.

The base electrolyte used in the experiments was 0.1 M $HClO_4$ + 4 × 10^{-4} M $AgClO_4$. In experiments where Pb was used as the mediator, 0.1 M Pb^{2+} was added to the base electrolyte as $Pb(ClO_4)_2$, and in experiments where Cu was used as the mediator, 10^{-3} M Cu^{2+} was added to the base electrolyte as $Cu(NO_3)_2$. All chemicals were Aldrich ultrapure reagents. Solutions were prepared with doubly distilled and "nanopure" (Barnstead) water. In the Pb (Cu) mediation experiments, a Pb (Ag) wire served as a reference electrode, and electrochemical potentials are reported with respect to the Pb/0.1 M Pb^{2+} (Ag/4 × 10^{-4} M Ag^+) reference electrode. In the experiments described below, the Ag^+ concentration in the electrolytes was chosen so that during growth the mass transport–limited current density was ~5 μA cm^{-2} (*24*). This allowed for a constant flux of Ag^+ as the electrochemical potential was cycled over a prescribed range during the mediation process. To observe the details of the growth process in situ, we had to use lower cycling frequencies than we typically use to grow a 100-nm-thick overlayer. After each of the experiments, Rutherford backscattering spectrometry and Auger electron spectroscopy sputter profiling were used to check for the concentration of the mediator in the Ag overlayer, and ion channeling was used to characterize the degree of overlayer/substrate epitaxy.

Figure 1 shows a time sequence of five images during DMG of Ag on Au(111) in the electrolyte 0.1 M $HClO_4$ + 4 × 10^{-4} M $AgClO_4$ + 0.1 M $Pb(ClO_4)_2$. The electrochemical potential was manually pulsed between 0.050 and 0.350 V (with respect to the Pb/0.1 M Pb^{2+} reference electrode). Figure 1A at 0.756 V shows the surface morphology just after the nucleation of Ag islands related to the formation of the second upd Ag layer. After this image was acquired, the voltage was changed to 0.350 V, allowing this layer to grow to near completion (Fig. 1B). During the acquisition of Fig. 1B, a 6-s potential pulse to 0.050 V [the Ag (111)/Pb^{2+} upd wave occurred at 0.138 V] seeded the third layer. Figure 1C acquired 74 s later shows the morphology that developed after a potential pulse to 0.050 V, which seeded a fourth layer. At this potential, there was a stable Pb upd layer on the surface. A potential pulse back to 0.350 V resulted in stripping of the Pb upd layer and continued growth of the third (now almost complete) and fourth Ag overlayers (Fig. 1D). Just after this image was captured, another 6-s potential pulse to 0.050 V was applied that seeded a fifth layer (Fig. 1E). Further growth was performed by retracting the STM tip from the sample surface in order to minimize a tip-shielding effect (*24*) and cycling the potential between 0.050 and 0.350 V at a frequency of 1.7 Hz. Figure 1F is a large-scan STM image showing the growth morphology of ~250 ML of Ag grown in this manner. The Ag overlayer was almost as flat as the original hydrogen flame–annealed Au(111) surface (*25*).

Figure 2 shows a time sequence of five images during DMG of Ag on Au(111) in the electrolyte 0.1 M $HClO_4$ + 4 × 10^{-4} M $AgClO_4$ + 10^{-3} M $Cu(NO_3)_2$. The potential was manually pulsed between −0.025 and −0.400 V (with respect to the Ag/4 × 10^{-4} M Ag^+ reference electrode). Because Cu does not underpotentially deposit on Ag, potential pulses to the region of Cu deposition (−0.400 V) were of short duration, and consequently we made no attempt to capture an image with Cu on the surface in these experiments. Just before the series of images shown in Fig. 2, about 150 ML of Ag were deposited on the Au(111) surface in the STM cell by cycling the potential between −0.025 and −0.400 V at 1.2 Hz. Figure 2A shows an atomically flat terrace region of the 150-ML-

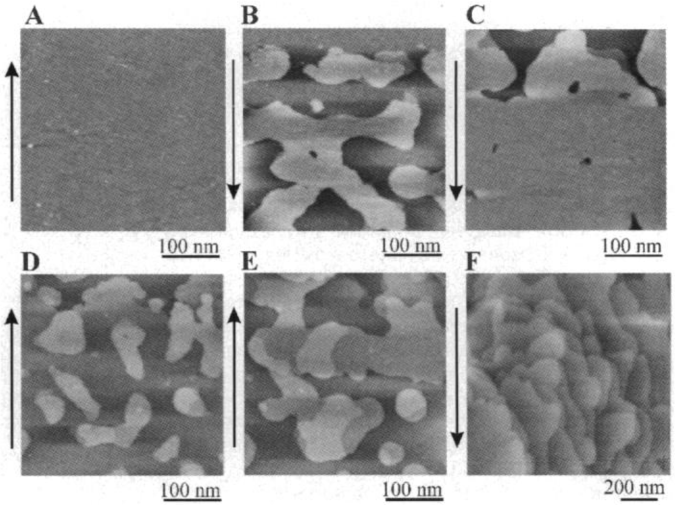

Fig. 2. (A to E) A time sequence of in situ STM images of Cu-mediated growth of Ag in the 0.1 M $HClO_4$ + 4 × 10^{-4} M $AgClO_4$ + 10^{-3} M $Cu(NO_3)_2$ electrolyte: (**A**) at 0 V, a flat terrace region of 150-ML Ag film on Au(111), 0 s; (**B**) after two short-duration voltage pulses that seeded the growth of 2 ML of Ag, 210 s; (**C**) 550 s; (**D**) after two voltage pulses that seeded the growth of two additional Ag layers, 655 s; and (**E**) 955 s. (**F**) A 250-ML-thick Ag overlayer on Au(111), at 0 V. Potentials are referenced to the Ag/4 × 10^{-4} M Ag^+ reference electrode. (B) and (E) were acquired at −0.025 V. Image acquisition time was 90 s. Arrows indicate the scan direction.

thick Ag overlayer. For typical DMG in this system (not performed in the STM), potential cycling is performed at frequencies of 1 to 5 Hz. Under these conditions several layers can be seeded before significant lateral layer growth. To simulate this situation in our in situ STM experiments, we used two potential pulses from −0.025 to −0.400 V 2 s in duration to seed the growth of two layers of Ag in close succession (Fig. 2B). Immediately after the pulsing small, isolated 2D Ag clusters nucleated and began to grow as 2-ML-high islands. Larger isolated Ag clusters, ~50 nm in diameter, were visible 20 s after the pulses, and at longer times (70 s) the 2-ML-high clusters began to merge. A 50-nm island diameter corresponds to the critical island size in this system for the transition to 3D cluster growth for the deposition conditions used (*26*). These Ag layers neared completion after about 550 s (Fig. 2C). At this stage, two square wave potential pulses 5 s apart were applied to the electrode, which resulted in the seeding of two additional Ag layers (Fig. 2D). Silver islands corresponding to the third and fourth layers are visible in this image. Figure 2E shows continued growth and merging of these islands. Figure 2F is a large-scan STM image showing the morphology of ~250 ML of Ag grown on the Au(111) surface with Cu as the mediator metal.

Ancillary in situ STM experiments were performed to ascertain the details of the mechanisms operating during DMG. We found that a upd Pb layer on Ag(111) behaves as a surfactant by promoting interlayer terrace exchange between deposited Ag adatoms and surfactant atoms. A high density (~10^{12} cm^{-2}) of 2D Ag nuclei forms under the Pb layer, presumably because rapid interlayer exchange minimizes intralayer adatom diffusion. This is analogous to UHV counterparts of surfactant-assisted growth (*27*). The other metal we chose as a mediator for this system was Cu, which does not undergo upd on Ag surfaces (*28*). The initial stage of Cu deposition on Ag(111) involves the formation of small (less than 1-nm diameter) 2D islands (density ~5×10^{10} cm^{-2}) that serve as attachment sites for Ag atoms. Because of the relative concentrations of Cu^{2+} and Ag^{+} in the electrolyte and the deposition scheme used, the transient deposition rate of Cu is about 40 times that of Ag, resulting in a significantly enhanced island nucleation density. On the basis of these observations, we suggest mechanisms for DMG as depicted in Fig. 3. In each case, mediation maintains a high density of 2D Ag nuclei on the surface, such that the average separation between nucleation centers is less than the critical island size.

Ion channeling was performed with a 2-MeV He^{2+} beam to characterize the Au(111) crystal before and after deposition of 120 nm of Ag on the Au(111) substrate by Pb and Cu DMG. The minimum yield (*29*) for channeling along the <111> (surface normal) direction for the flame-annealed gold crystal was 10%. The yield (*30*) associated with the Ag peak both for Pb and Cu mediation was ~20 and 10%, respectively, for channeling along the <111> and <110> direction. These results are indicative of an epitaxial Ag single-crystal overlayer. Rutherford backscattering spectrometry and Auger electron spectroscopy sputter-depth profiling showed no traces of mediator metal in the Ag film (*31*).

Our study shows that UHV-derived concepts can be used in electrodeposition to deposit high-quality heteroepitaxial metallic thin films. Additionally, we have taken advantage of the enhanced nucleation provided by the DMG technique in several applications that are difficult because of seeding problems. These include the plating of Cu onto a patterned TiN-coated Si(100) substrate, and the deposition of Co on n-type Si(100) (*32*).

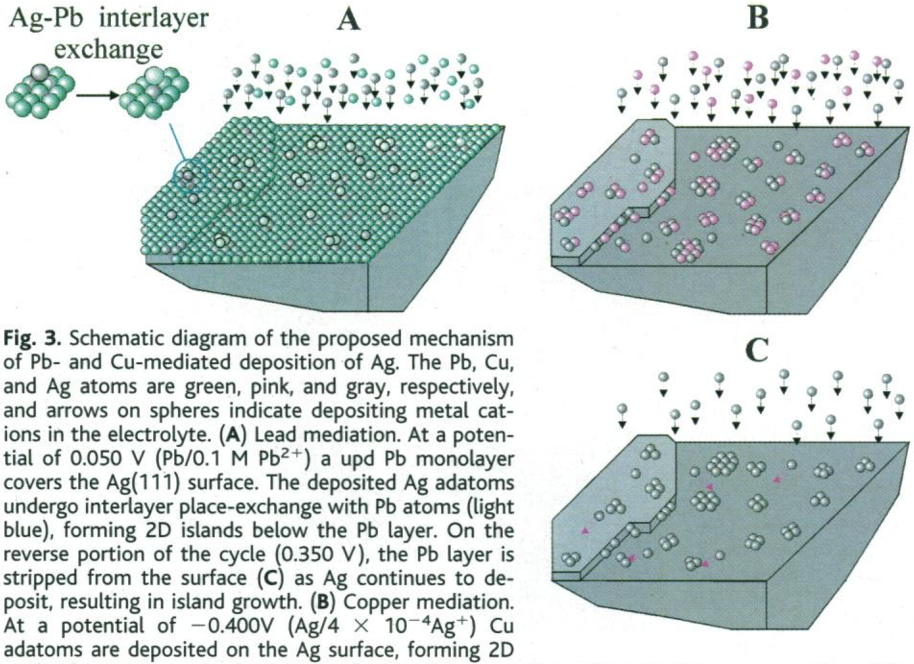

Fig. 3. Schematic diagram of the proposed mechanism of Pb- and Cu-mediated deposition of Ag. The Pb, Cu, and Ag atoms are green, pink, and gray, respectively, and arrows on spheres indicate depositing metal cations in the electrolyte. (**A**) Lead mediation. At a potential of 0.050 V (Pb/0.1 M Pb^{2+}) a upd Pb monolayer covers the Ag(111) surface. The deposited Ag adatoms undergo interlayer place-exchange with Pb atoms (light blue), forming 2D islands below the Pb layer. On the reverse portion of the cycle (0.350 V), the Pb layer is stripped from the surface (**C**) as Ag continues to deposit, resulting in island growth. (**B**) Copper mediation. At a potential of −0.400V (Ag/4 × $10^{-4}Ag^{+}$) Cu adatoms are deposited on the Ag surface, forming 2D nuclei that serve as attachment sites for Ag adatoms on the surface. On the reverse portion of the cycle (−0.025 V), Cu is selectively stripped from the surface (C), causing the Ag-Cu islands to decompose into 2D Ag islands that serve as growth centers as Ag continues to deposit.

References and Notes

1. Z. Zhang and M. G. Legally, *Science* **276**, 377 (1997).
2. W. Plieth, *Electrochim. Acta* **37**, 2115 (1992).
3. D. R. Gabe, *Principles of Metal Surface Treatment and Protection* (Pergamon, Oxford, ed. 2, 1978), pp. 29–79.
4. R. J. Nichols, W. Beckmann, H. Meyer, N. Batina, D. M. Kolb, *J. Electroanal. Chem.* **330**, 381 (1992).
5. O. M. Magnussen, F. A. Moller, A. Lachenwitzer, R. J. Behm, in *Electrochemical Synthesis and Modification of Materials*, Materials Research Society Symposium vol. 451, Boston, MA, 2 to 5 December 1996; P. C. Andricacos, S. G. Corcoran, J.-L. Delplancke, T. P. Moffat, P. C. Searson, Eds. (Materials Research Society, Pittsburgh, PA, 1997), pp. 43–48.
6. D. M. Kolb, R. J. Randler, R. I. Wielgosz, J. C. Ziegler, in (*5*), pp. 19–30.
7. M. Dietterle, T. Will, D. M. Kolb, *Surf. Sci.* **396**, 189 (1998).
8. G. Rosenfeld, R. Servaty, C. Teichert, B. Poelsema, G. Comsa, *Phys. Rev. Lett.* **71**, 895 (1993).
9. H. A. van der Vegt, H. M. van Pinxteren, M. Lohmeier, E. Vlieg, J. M. C. Thornton, *ibid.* **68**, 3335 (1992).
10. J. Tersoff, A. W. Denier van der Gon, R. M. Tromp, *ibid.* **72**, 266 (1994).
11. Z. Zhang and M.G. Lagally, *ibid.*, p. 693.
12. J. A. Meyer, J. Vrijmoeth, H. A. van der Vegt, E. Vlieg, R. J. Behm, *Phys. Rev. B* **51**, 14790 (1995).
13. S. Harris, *ibid.* **52**, 16793 (1995).
14. In overlayer/substrate systems displaying 2D growth for more than just several monolayers, the growth is never truly one layer at a time. Instead, there are several layers growing laterally at the same time in a stable mode. Three-dimensional cluster growth can develop because of an instability, possibly of the Mullins-Sekerka type. See, for example, A. Mazor, D. J. Srolovitz, P. S. Hagan, B. J. Bukiet, *Phys. Rev. Lett.* **60**, 424 (1988).
15. G. Ehrlich and F. G. Hudda, *J. Chem. Phys.* **44**, 1039 (1966).
16. R. L. Schwoebel and E. J. Shipsey, *J. Appl. Phys.* **37**, 3682 (1966).
17. L.-H. Tang, *J. Phys. I France* **3**, 935 (1993).
18. K. Sieradzki, Provisional U.S. Patent Application S/N 60/077, 476 (March 1998).
19. We performed a series of control experiments in the base electrolyte (no mediator) under otherwise identical growth conditions as those used during DMG. Three-dimensional cluster growth developed in all experiments for these systems.
20. S. G. Corcoran, G. S. Chakarova, K. Sieradzki, *Phys. Rev. Lett.* **71**, 1585 (1993).
21. D. M. Kolb, in *Advances in Electrochemistry and Electrochemical Engineering*, H. Gerischer and C. W. Tobias, Eds. (Wiley, New York, 1978), pp. 125–271.
22. H. Bort, K. Juttner, W. J. Lorenz, E. Schmidt, *J. Electroanal. Chem.* **90**, 413 (1978).
23. W. Obretenov *et al.*, *J. Electrochem. Soc.* **140**, 692 (1993).
24. While the measured electrochemical current density corresponding to Ag deposition in the experiment was ~ 5 μA cm^{-2}, the deposition rate as determined by STM coverage measurements was almost a factor of 5 less. This undoubtedly resulted from tip-shielding effects that other researchers have also noted. See, for example, D. M. Kolb, R. Ullmann, T. Will, *Science* **275**, 1097 (1997).
25. The STM was used to determine the root mean

square surface roughness (*R*) of Au surfaces and Ag overlayers as a function of scan size after DMG of ~250 ML of Ag. After H_2 flame annealing of the Au(111) surface, *R* over a 5 μm by 5 μm area was typically in the range of 0.275 to 0.340 nm. After DMG, *R* was determined for the Ag overlayer (for example, over a 5 μm by 5 μm area, R = 0.336 nm) and the Au surface over the identical area (for example, R = 0.392 nm) by electrochemically stripping the layer in situ. The larger *R* of the Au surfaces after stripping of the Ag layer is related to submonolayer roughness that developed from surface alloying [S. G. Corcoran, G. S. Chakarova, K. Sieradzki, *J. Electroanal. Chem.* **337**, 85 (1994)].

26. The deposition current used corresponds to a flux of 3.1×10^{13} atoms cm^{-2} s^{-1} (0.02 ML s^{-1}). J. D. Porter and T. O. Robinson [*J. Phys. Chem.* **97**, 6696 (1993)] reported a value of 1.4×10^{-6} cm^{-2} s^{-1} for the diffusivity of Ag adatoms on Ag(111) in electrolytes. Calculating the value of $(4a^2D/J)^{1/6}$, we obtained 50 nm as an order of magnitude estimate of the critical island size for our growth conditions.
27. J. Camarero *et al.*, *Phys. Rev. Lett.* **81**, 850 (1998).
28. M. Dietterle, T. M. Will, D. M. Kolb, *Surf. Sci.* **342**, 29 (1995).
29. L. C. Feldman, J. W. Mayer, S. T. Picraux, *Materials Analysis by Ion Channeling* (Academic Press, New York, 1982), pp. 44–46.
30. The yield was determined as the area ratio of the Ag peaks for random alignment and the channeling alignment.
31. The sensitivity of Auger electron spectroscopy and Rutherford backscattering spectrometry is of order 0.5 and 1 atomic %, respectively. See, for example, M. P. Seah and D. Briggs, in *Practical Surface Analysis*, D. Briggs and M. P. Seah, Eds. (Wiley, New York, ed. 2, 1990), vol. 1, chap. 1.
32. K Sieradzki, S. R. Brankovic, N. Dimitrov, unpublished data.

33. We thank B. Wilkens and R. Culbertson for assistance with the Rutherford backscattering spectrometry measurements and gratefully acknowledge the support of this work by the NSF, Division of Materials Research (contract DMR-9510663).

27 October 1998; accepted 26 February 1999

Strongly Photonic Macroporous Gallium Phosphide Networks

Frank J. P. Schuurmans,[1]* Daniël Vanmaekelbergh,[2]
Jao van de Lagemaat,[2]† Ad Lagendijk[1]

A photo-assisted electrochemical etching technique to fabricate macropores in single-crystalline gallium phosphide (GaP) with variable porosity has been developed. Scanning electron microscopy and x-ray diffraction experiments confirm that the material consists of three-dimensional, interconnected random networks with pore sizes of about 150 nanometers. Optical transmission measurements demonstrate that the nonabsorbing disordered structures strongly scatter light. The photonic strength is controlled by filling the pores with liquids of different refractive indices. Macroporous gallium phosphide filled with air has the highest scattering efficiency for visible light.

In a binary system with components of refractive indices n_1 and n_2, the efficiency of light scattering depends on how these components are organized in the system, the dimensions of the components, and the refractive index ratio $n_1/n_2 = m$. Scattering of light is strongest if m is large and the length scale of refractive index variation, s, is comparable to the wavelength of light λ. This regime has received much attention in the search for strongly scattering (photonic) materials. For ordered systems with a periodic variation in the refractive index, that material is a photonic crystal. Such crystals feature photonic band gaps (*1*, *2*): frequency ranges for which light will not propagate in the crystal because of multiple Bragg reflections. If the material is disordered, the interference of scattered light ultimately leads to Anderson localization (*3*, *4*). Photonic band gaps and Anderson localization are closely related. Both inhibit light propagation due to interference (not absorption) and can only be obtained for strongly photonic materials, those with $m \sim 3$ or larger.

For infrared light, Anderson localization has been reported for gallium arsenide powders ($m \simeq 3.5$) (*4*), and a two-dimensional (2D) photonic band gap has been reported for macroporous Si ($m \simeq 3.4$) (*5*). In the visible, considerable progress has been made by the preparation of 3D air-sphere crystals of TiO_2 ($m \simeq 2.7$) (*2*). Inhibition of the propagation of visible light has not yet been reported for 3D structures—apparently larger values of m (>2.7) are needed. Obviously, m is a crucial parameter for photonic materials. In addition to large m, it is thus desirable to have the ability to tune m, allowing investigation of its importance for the photonic strength.

We report here on the optical scattering properties of electrochemically etched, macroporous, single-crystalline gallium phosphide (GaP). The 3D random network of GaP is completely interconnected, as observed by scanning electron microscopy (SEM) and confirmed by x-ray diffraction. An important consequence of the macroporous network is that we are able to modify the refractive index ratio by filling the voids with materials with different refractive indices without disturbing the overall porous structure. GaP has a large refractive index of ~3.3 and an indirect band gap of 2.24 eV (550 nm) (*6*), which allows the preparation of strongly photonic systems ($m \simeq 3.3$) with negligible absorption in the red part of the visible spectrum. Using an etching technique, we prepared slabs of strongly scattering, random GaP networks with structural units of about 150 nm and two different porosities, 35 and 50%. Furthermore, the method makes it possible to control the thickness of the scattering slab.

The macroporous GaP structure is formed by anodic etching of n-type GaP single crystals (donor density, 2×10^{17} cm^{-3}) under dielectric breakdown conditions (*7*–*9*). The 350-μm-thick polished wafers are mounted with a (100) face exposed to the 0.5 M H_2SO_4 electrolyte. Application of a strong positive potential (15 V versus normal hydrogen electrode) leads to severe band bending at the n-GaP/electrolyte interface. Interband tunneling of electrons (*10*) from the valence band or from band gap states to the conduction band takes place, generating holes at the surface, which are consumed in anodic dissolution of the GaP. The generation of holes is spatially nonuniform, which results in the porous network growing deeper into the GaP crystal. The anodic charge is proportional to the thickness of the porous structure L, enabling coulometric control of this important parameter (*9*). A SEM micrograph of a cross section of the porous slab is used to calibrate the linear charge-thickness relation. The porosity is determined to be ~35 volume % of air. We prepared a series of samples with porous slab thicknesses ranging from 5 to 120 μm.

In addition to the anodically etched GaP (A-GaP), we also prepared photoanodically etched GaP (PA-GaP) samples. Exploiting a technique that uses homogeneous photo-assisted etching, we are able to prepare slabs with a higher porosity. A-GaP samples are subjected to a further process of photoanodic etching in a H_2O:H_2SO_4:H_2O_2 electrolyte solution, using 50 mW of 1.96-eV sub–band gap light from a HeNe laser. Photons are absorbed by a transition of an electron from the top of the valence band to an interfacial state, 0.3 eV below the conduction band, followed by thermal release of the interfacial electron into the conduction band (*11*). The remaining hole is involved in anodic dissolution. Because of the weak absorption of the light in the porous structure, the etch rate is

---

[1] Van der Waals-Zeeman Instituut, Universiteit van Amsterdam, Valckenierstraat 65, 1018 XE Amsterdam, The Netherlands. [2] Debye Instituut, Universiteit Utrecht, Post Office Box 80000, 3508 TA Utrecht, The Netherlands.

*To whom correspondence should be addressed. E-mail: schuurma@phys.uva.nl

†Present address: Basic Sciences Center, National Renewable Energy Laboratory, 1617 Cole Boulevard, Golden, CO 80401–3393, USA.